MODELING THE BENCHMARK ACTIVE CONTROL TECHNOLOGY WIND-TUNNEL MODEL FOR APPLICATION TO FLUTTER SUPPRESSION

Martin R. Waszak,* *NASA Langley Research Center, Hampton, Virginia*

Abstract

This paper describes the formulation of a model of the dynamic behavior of the Benchmark Active Controls Technology (BACT) wind-tunnel model for application to design and analysis of flutter suppression controllers. The model is formed by combining the equations of motion for the BACT wind-tunnel model with actuator models and a model of wind-tunnel turbulence. The primary focus of this paper is the development of the equations of motion from first principles using Lagrange's equations and the principle of virtual work. A numerical form of the model is generated using values for parameters obtained from both experiment and analysis. A unique aspect of the BACT wind-tunnel model is that it has upper- and lower-surface spoilers for active control. Comparisons with experimental frequency responses and other data show excellent agreement and suggest that simple coefficient-based aerodynamics are sufficient to accurately characterize the aeroelastic response of the BACT wind-tunnel model. The equations of motion developed herein have been used to assist the design and analysis of a number of flutter suppression controllers that have been successfully implemented.

Introduction

Active control of aeroelastic phenomena, especially in the transonic speed regime, is a key technology for future aircraft design.[1] The Benchmark Active Controls Technology (BACT) project is part of NASA Langley Research Center's Benchmark Models Program[1,2] for studying transonic aeroelastic phenomena. The BACT wind-tunnel model was developed to collect high quality unsteady aerodynamic data (pressures and loads) near transonic flutter conditions and demonstrate flutter suppression using spoilers. Accomplishing these objectives required the design and implementation of active flutter suppression. The multiple control surfaces and sensors on the BACT enabled the investigation of multivariable flutter suppression. And the availability of truly multivariable control laws provides an opportunity to evaluate the effectiveness of a controller performance evaluation (CPE) tool[3] used to assess open- and closed-loop stability and controller robustness when applied to multivariable systems. An underlying requirement of all these objectives is the availability of a mathematical model of the BACT dynamics.

A mathematical model is the basis for nearly all control design methods, therefore an appropriate model is essential. The importance of having a good model of the dynamic behavior cannot be overstated and the model must be developed with a mind toward the needs of control law design. In addition, appropriate models are required to accurately assess system performance and robustness. Extensive analysis and simulation are usually required before controller implementation to assure that safety is not compromised. This is especially true in the area of aeroservoelastic testing in which failure can result in destruction of the wind-tunnel model and damage to the wind-tunnel.

Mathematical models for control law synthesis must characterize the salient dynamic properties of the system. One of the most important properties to accurately model is the frequency response in the vicinity of the key dynamics over the anticipated range of operating conditions. In the case of flutter suppression, the key dynamics occur near the flutter frequency and the operating conditions correspond to a wide range of dynamic pressures and Mach numbers representing both stable and unstable conditions. Also important are the key parametric variations associated with the system and the uncertainties associated with the assumptions and limitations of the analysis tools and other data used to build the model.

The development of the model of the dynamic behavior of the BACT presented herein was motivated by several factors. A primary motivation was based on the fact that the tool normally used at NASA Langley to model aeroelastic systems, ISAC[4], is unable to model spoilers. Since the demonstration of flutter suppression using spoilers was a key objective of the BACT project an alternative modeling approach was needed. Another motivation for the particular modeling approach taken here was the desire to assess the impact of model uncertainty and parametric

* Aerospace Research Engineer, Senior Member AIAA.

variations on control system design, performance, and robustness.

By developing the model from first principles using appropriate idealizations of the structural and aerodynamic characteristics, a model was developed that includes spoiler controls and explicitly contains the key physical parameters. The analytical and parametric nature of the model also provides physical insights not readily obtained from purely numerical models (such as those produced by ISAC and similar tools). While this paper emphasizes the development of the equations of motion of the BACT wind-tunnel model, a complete model is presented including actuator and turbulence models, and validation of the resulting numerical model.

The BACT Wind-Tunnel Model

The BACT wind-tunnel model is a rigid, rectangular, wing with an NACA 0012 airfoil section.[5] A drawing of the model is shown in Figure 1. It is equipped with a trailing-edge control surface, and upper- and lower-surface spoilers that can be controlled independently via hydraulic actuators. The wind-tunnel model is instrumented with pressure transducers, accelerometers, control surface position sensors, and hydraulic pressure transducers. The accelerometers are the primary sensors for feedback control and are located at each corner of the wing.

The wing is mounted to a device called the Pitch and Plunge Apparatus[5] (PAPA) which is designed to permit motion in principally two modes -- rotation (or pitch), and vertical translation (or plunge). A drawing of the PAPA is shown in Figure 2. The mass, inertia, and center of gravity location of the system can be controlled by locating masses at various points along the mounting bracket. The stiffness properties can be controlled by changing the properties of the rods. The PAPA is instrumented with strain gauges to measure normal force and pitching moment and is mounted to a turntable that can be rotated to control the wing angle of attack.

The combination of the BACT wing section and PAPA mount will be referred to as the BACT system. The BACT system was precisely tuned to flutter within the operating range of the Transonic Dynamics Tunnel (TDT)[6] at NASA Langley Research Center in which the system was tested. The range of Mach numbers and dynamic pressures over which flutter occurs permits the study of transonic aeroelastic phenomena. More detailed descriptions of both the BACT wing section and the PAPA mounting system can be found in References 5 and 7.

The BACT system has dynamic behavior very similar to the classical two degree-of-freedom (2-DOF)

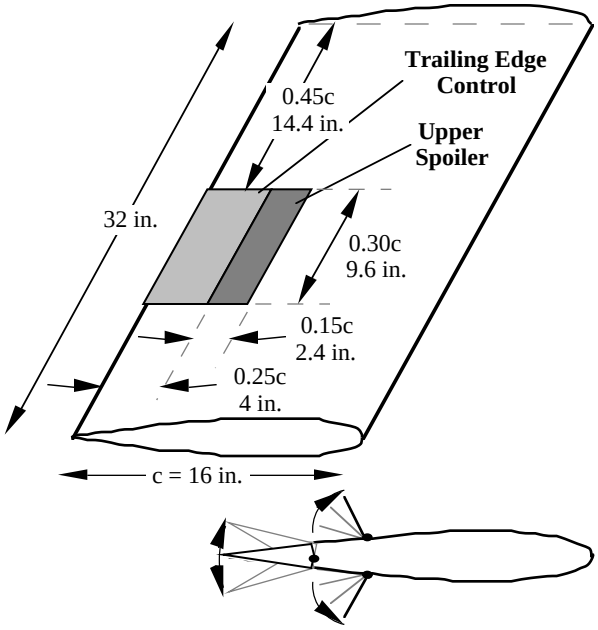

Figure 1 - BACT Wing Section Diagram

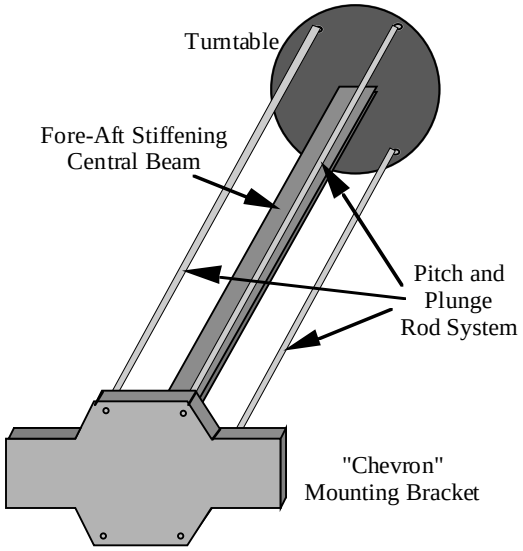

Figure 2 - PAPA Diagram

problem in aeroelasticity.[8] The difference is primarily the complexity of aerodynamic behavior and presence of additional structural modes. The finite span and low aspect ratio of the BACT wing introduce significant three dimensional flow effects. Higher frequency structural degrees of freedom are associated with the PAPA mount and the fact that the wing section is not truly rigid.

The control surfaces also introduce complexities not typically reflected in the classical 2-DOF system. The mass and inertia of the control surfaces and potential flexibility in their support structures introduce inertial coupling effects. The finite span of the control

surfaces and their close proximity to each other also introduce significant aerodynamic effects. All these issues influence the development of the equations of motion but, as will be seen, do not force the abandonment of the 2-DOF system structure.

Aeroelastic Equations of Motion

Lagrange's equations were used to derive the equations of motion for the BACT system and the principle of virtual work was used to obtain expressions for viscous damping and the generalized aerodynamic forces. Lagrange's equations and the principle of virtual work provide a simple and straight forward method for deriving the equations of motion for aeroelastic systems.[9] Lagrange's equations readily allow one to represent motions relative to a moving frame. The principle of virtual work has the advantage of automatically accounting for the forces of constraint and thereby greatly simplifying the determination of generalized forces.

The basic requirement for applying Lagrange's equations is that the velocity of each point in the body be represented in an inertial frame. The efficient application of Lagrange's equations can be facilitated by representing the inertial quantities in convenient coordinate systems and selecting an appropriate set of generalized coordinates.

Coordinate Axes and Generalized Coordinates

The BACT system can be idealized as a collection of four rigid bodies corresponding to each of the three control surfaces and the remaining wing/PAPA element. Figure 4 depicts the relevant quantities for the wing and the trailing edge control surface. The spoiler control surfaces were treated in an analogous fashion but are omitted here for ease of discussion.

There were essentially five coordinate systems used. One coordinate system is fixed to the wing, moving with it. Another coordinate system is fixed in inertial space and oriented relative to the turntable to which the BACT system was mounted. It was chosen to coincide with the undeformed position of the body-fixed system. The three others are fixed to each of the control surfaces and rotated relative to the body-fixed system about the hinge of each surface.

The origin of the inertial coordinate axes is located at the shear center of the undeformed position. The origin of the body fixed coordinate axes coincides with the instantaneous shear center of the system. The origin of the control surface-fixed coordinate axes coincide with the hinge lines.

The generalized coordinates were selected to simplify the derivation of the equations of motion. Their selection is based on some key assumptions about the

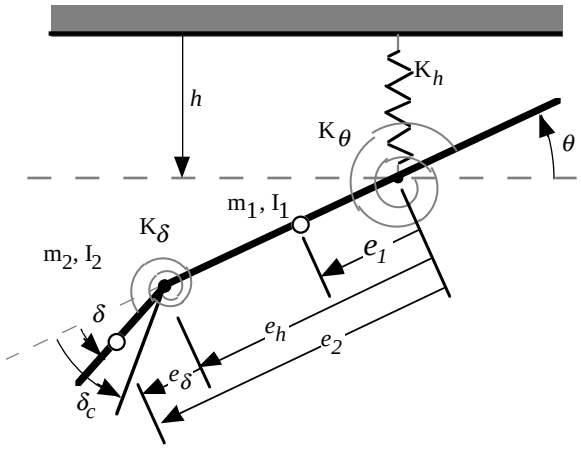

Figure 4 - Structural representation showing trailing edge control only.

nature of the motion of the BACT system. The wing section and each control surface are assumed to be rigid in both the spanwise and chordwise directions. This assumption is supported by the fact that the wing and control surfaces were constructed to be as rigid as possible.

It is also assumed that the motion is limited to two degrees of freedom -- pitch and plunge. This assumption implies that the other structural modes of the BACT system are insignificant. Investigation of the structural vibration characteristics of the PAPA mount with a very similar wing model was shown to support this assumption.[10] The next lowest frequency for any transverse mode was more than six times the frequency of the pitch and plunge modes and well outside the frequency range of interest.

Based on these assumptions the BACT requires five generalized coordinates, two associated with the pitch and plunge degrees of freedom of the entire wing and three are associated with the angular rotation of the control surfaces. The five generalized coordinates therefore are pitch angle, θ, and plunge displacement, h, of the body fixed coordinate axes relative to the inertial coordinate axes and the trailing edge, upper-, and lower-spoiler control surface angles, δ_{TE}, δ_{US}, and δ_{LS}, respectively. The three coordinates, h, θ, and $\delta \equiv \delta_{TE}$, for the system including only the trailing edge control surface are depicted in Figure 4.

The relation between the generalized coordinates and the angle of attack of the wind-tunnel model will be important in formulating the generalized aerodynamic forces later. Based on the choice of the generalized coordinates the following expression can be used to determine the angle-of-attack.

$$\alpha(x,y,t) = \theta_T + \theta(t) + \frac{\dot{h}(t)}{U_0} + \frac{\ell(x)\dot{\theta}(t)}{U_0} - \frac{w_g(x,y,t)}{U_0} \quad (1)$$

where θ_T is the turntable angle, $\ell(x)$ is the distance from the origin of body fixed coordinate system to the angle of attack reference, x (positive aft), w_g is the normal perturbation velocity of the local flow field (positive down relative to the free stream flow), and U_0 is the freestream velocity.

Kinetic and Potential Energy

The selection of the generalized coordinates allows expressions for the kinetic and potential energies to be formulated. The kinetic energy of the BACT system is the sum of the kinetic energy of the wing and the three control surfaces.

The kinetic energy of a body is the work required to increase its velocity from rest to some value relative to an inertial frame. Using the quantities defined in Figure 4 the kinetic energy expression for the BACT system including only the trailing edge control can be written

$$\begin{aligned} T = {} & \frac{1}{2} m_1 (\dot{h} + e_1 \dot{\theta})^2 + \frac{1}{2} I_1 \dot{\theta}^2 \\ & + \frac{1}{2} m_2 (\dot{h} + e_2 \dot{\theta} + e_\delta \dot{\delta})^2 + \frac{1}{2} I_2 (\dot{\theta} + \dot{\delta})^2 \end{aligned} \quad (2)$$

The potential energy of a rigid body consists of two terms, the strain energy and the gravitational potential energy. The gravitational potential is defined relative to a datum, usually the origin of the inertial reference frame. Using the quantities defined in Figure 4 and assuming the datum to be the origin of the inertial frame the gravitational potential for the BACT system is

$$\begin{aligned} U_g = {} & -m_1 g (h + e_1 \sin\theta) \cos\theta_T \\ & -m_2 g (h + e_2 \sin\theta + e_\delta \sin\delta) \cos\theta_T \end{aligned} \quad (3)$$

where g is the gravitational acceleration.

The strain energy is the work done in going from the undeformed reference position to the deformed position. Using the quantities defined in Figure 4 the strain energy for the BACT system is

$$U_e = \frac{1}{2} K_h h^2 + \frac{1}{2} K_\theta \theta^2 + \frac{1}{2} K_\delta (\delta_c - \delta)^2 \quad (4)$$

where K_h and K_θ are the spring constants associated with the stiffness properties of the PAPA mount and where K_δ is the spring constant representing the flexibility in the structure supporting the actuator. Note that the strain energy associated with the control surface is based on the difference between the commanded and the actual control surface rotation, δ_c and δ, respectively.

The total potential energy for the BACT system is simply the sum of the gravitational potential and the strain energy, Eqns (3) and (4), respectively.

Applying Lagrange's Equations

Lagrange's equations can be expressed in the following form.

$$\frac{d}{dt}\left(\frac{\partial T}{\partial \dot{q}_i}\right) - \frac{\partial T}{\partial q_i} + \frac{\partial U}{\partial q_i} = Q_{q_i} \quad (5)$$

where the T and U are the kinetic and potential energy of the system, respectively, q_i is the ith generalized coordinate, and Q_{q_i} is the generalized force associated with q_i and includes externally applied forces, nonconservative forces, and forces of constraint.

Applying the expressions for the kinetic and potential energies to Eqn (5) results in the following system of equations.

$$\begin{aligned} & \begin{bmatrix} m & s_{h\theta} & s_{h\delta} \\ s_{h\theta} & I_\theta & s_{\theta\delta} \\ s_{h\delta} & s_{\theta\delta} & I_\delta \end{bmatrix} \begin{Bmatrix} \ddot{h} \\ \ddot{\theta} \\ \ddot{\delta} \end{Bmatrix} + \begin{bmatrix} K_h & 0 & 0 \\ 0 & K_\theta & 0 \\ 0 & 0 & K_\delta \end{bmatrix} \begin{Bmatrix} h \\ \theta \\ \delta \end{Bmatrix} \\ & = \begin{Bmatrix} 0 \\ 0 \\ K_\delta \end{Bmatrix} \delta_c + \begin{Bmatrix} m \\ s_{h\theta} \cos\theta \\ s_{h\delta} \cos\delta \end{Bmatrix} g \cos\theta_T + \begin{Bmatrix} Q_h \\ Q_\theta \\ Q_\delta \end{Bmatrix} \end{aligned} \quad (6)$$

The terms m, I_θ, and I_δ are the generalized masses of the pitch, plunge, and control surface modes, respectively. The terms $s_{h\theta}$, $s_{h\delta}$, and $s_{\theta\delta}$ are the inertial coupling between the various degrees-of-freedom. These terms are related to the quantities defined in Figure 4 by the following relations.

$$\begin{aligned} m &\equiv m_1 + m_2 & s_{h\theta} &\equiv m_1 e_1 + m_2 e_2 \\ I_\theta &\equiv I_1 + I_2 + m_1 e_1^2 + m_2 e_2^2 & s_{h\delta} &\equiv m_2 e_\delta \\ I_\delta &\equiv I_2 + m_2 e_2^2 & s_{\theta\delta} &\equiv I_2 + m_2 e_2 e_\delta \end{aligned} \quad (7)$$

If one assumes that the control surface stiffness is very large, (i.e., the deformation due to hinge load is insignificant) then Eqn (6) can be simplified by eliminating the generalized force associated with the control surface, Q_δ.

Assume that the control surface stiffness is very large so that

$$K_\delta \approx \frac{1}{\varepsilon}, \quad \varepsilon << 1$$

Eqn (6) can now be approximated by the following equations after eliminating terms of order ε.

$$\delta = \delta_c \tag{8}$$

$$\begin{bmatrix} m & s_{h\theta} \\ s_{h\theta} & I_\theta \end{bmatrix} \begin{Bmatrix} \ddot{h} \\ \ddot{\theta} \end{Bmatrix} + \begin{bmatrix} K_h & 0 \\ 0 & K_\theta \end{bmatrix} \begin{Bmatrix} h \\ \theta \end{Bmatrix} = -\begin{Bmatrix} s_{h\delta} \\ s_{\theta\delta} \end{Bmatrix} \ddot{\delta} + \begin{Bmatrix} m \\ s_{h\theta} \end{Bmatrix} g \cos\theta_T + \begin{Bmatrix} Q_h \\ Q_\theta \end{Bmatrix} \tag{9}$$

Note that the value of θ has been assumed to be small so that $\cos\theta$ is approximately unity. Also note that the inertial coupling between the wing structure and the control surface is retained in the equations.

All that remains to complete the equations of motion is to determine expressions for the generalized forces, Q_h and Q_θ.

Applying the Principle of Virtual Work

The principle of virtual work can be applied to obtain expressions for generalized forces. The basic advantage of using this method is that the forces of constraint are eliminated automatically. In addition, the principle of virtual work can be used to determine expressions for dissipative forces such as damping.

The generalized force, Q_{q_i}, can be determined from the following equation.

$$Q_{q_i} = \frac{\partial \delta W}{\partial \delta q_i} \tag{10}$$

where δW is the work done on the system by an arbitrary infinitesimal (or *virtual*) displacement of the generalized coordinates. This *virtual* work includes the work done by nonconservative forces (e.g., damping) and external forces. The work done by forces of constraint are zero under virtual displacements.

Nonconservative (Damping) Forces

Structural damping is often characterized as a viscous force. Experimental data suggests that this is a reasonable assumption for the BACT system undergoing small motions. Viscous forces are those where the force varies in proportion to the velocity at the point the force is applied but in the opposite direction. The following expression was derived to represent the generalized damping forces for the BACT.

$$\begin{Bmatrix} Q_h{}^{nc} \\ Q_\theta{}^{nc} \end{Bmatrix} = -\begin{bmatrix} m & s_{h\theta} \\ s_{h\theta} & I_\theta \end{bmatrix} \begin{bmatrix} 2\zeta_h\omega_h & 0 \\ 0 & 2\zeta_\theta\omega_\theta \end{bmatrix} \tag{11}$$

The constant terms in Eqn (11) were chosen so that the damping coefficients associated with the plunge and pitch modes, ζ_h and ζ_θ, respectively, correspond to those obtained from experiment. The matrix premultiplying the diagonal damping matrix is the mass matrix from Eqn (9). The other constants, ω_h and ω_θ, correspond to the in vacuo vibration frequencies for the pitch and plunge modes.

External (Aerodynamic) Forces

The externally applied forces are due to aerodynamics and result from the distributed pressures applied to the surface of the BACT wing. For the wing the virtual work can be written

$$\delta W = \int_0^b \int_{-c/2}^{+c/2} p(x,y,t)\, \delta z(x,y,t)\, dx\, dy \tag{12}$$

where b is the wing semi-span, c is the section chord, $p(x,y,t)$ is the differential pressure distribution over the surface of the wing, and $\delta z(x,y,t)$ is a virtual displacement normal to the wing surface. Figure 5 depicts the pressure distribution for a chordwise section.

The virtual displacement can be written in terms of virtual displacements of the generalized coordinates h, θ, and δ as follows.

$$-\delta z(x,y,t) = \delta h(t) + (x - x_p)\delta\theta(t) + \begin{cases} 0, & x < x_f \\ (x - x_f)\delta\delta, & x > x_f \end{cases} \tag{13}$$

Substituting this expression in Eqn (12) and performing the differentiation described in Eqn (10) results in the following expressions for the generalized aerodynamic forces.

$$\begin{aligned} Q_h &= \frac{\partial \delta W}{\partial \delta h} \\ &= -\int_0^b \int_{-c/2}^{+c/2} p(x,y,t)\, dx\, dy \equiv -L \\ Q_\theta &= \frac{\partial \delta W}{\partial \delta \theta} \\ &= -\int_0^b \int_{-c/2}^{+c/2} p(x,y,t)(x - x_p)\, dx\, dy \equiv M_p \\ Q_\delta &= \frac{\partial \delta W}{\partial \delta \delta} \\ &= -\int_0^b \int_{x_f}^{+c/2} p(x,y,t)(x - x_f)\, dx\, dy \equiv H_\delta \end{aligned} \tag{14}$$

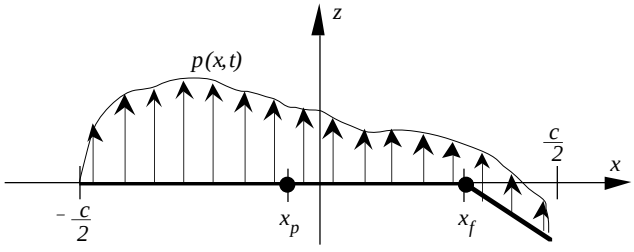

Figure 5 - Pressure distribution over wing section.

Where L, M_p, and H_δ are the lift, pitching moment about the reference point, x_p, and the control surface moment about its hinge-line, respectively. The reference point, x_p, was chosen to correspond to the shear center (i.e., the origin of the body fixed coordinate system).

There are several ways in which the integrated surface pressures can be approximated in practice. If computational aerodynamic analysis results are available the integration can be approximated by using the pressures on the computational grid. If experimental force and moment data are available it can be used directly allowing for potential differences in the moment reference point.

A common method of approximating the aerodynamic forces is to use stability and control derivatives. The aerodynamic forces are represented as a linear function of angle-of-attack and control surface deflection and their rates as shown in Eqns (15) and (16). Descriptions of each coefficient are presented below in Table 2. A comparable expression for the hinge moment has been omitted since the need for the generalized force associated with hinge moment in the equations of motion was eliminated in Eqn (9).

$$\begin{aligned} L &= qSC_L \\ &= qS\Big[C_{L_0} + C_{L_\alpha}\alpha + C_{L_\delta}\delta \\ &\quad + \frac{\bar{c}}{2U_0}\left(C_{L_{\dot\alpha}}\dot\alpha + C_{L_q}\dot\theta + C_{L_{\dot\delta}}\dot\delta\right)\Big] \end{aligned} \tag{15}$$

$$\begin{aligned} M_p &= qS\bar{c}C_M \\ &= qS\bar{c}\Big[C_{M_0} + C_{M_\alpha}\alpha + C_{M_\delta}\delta \\ &\quad + \frac{\bar{c}}{2U_0}\left(C_{M_{\dot\alpha}}\dot\alpha + C_{M_q}\dot\theta + C_{M_{\dot\delta}}\dot\delta\right)\Big] \end{aligned} \tag{16}$$

The coefficient-based approach is a rather simplistic way to represent the aerodynamic forces and moments, but it is quite acceptable for the BACT system as will be seen. The need to include more sophisticated aerodynamic modeling approaches such as rational function approximations or time accurate CFD is mitigated by the fact that the reduced frequency for the BACT system is relatively low, approximately 0.044.

Using the expression for angle-of-attack from Eqn (1) in Eqns (15) and (16) the expression for the generalized applied external forces in Eqn (17) can be obtained.

$$\begin{aligned} \begin{Bmatrix} Q_h{}^e \\ Q_\theta{}^e \end{Bmatrix} &= qS\begin{bmatrix} -C_{L_0} \\ \bar{c}C_{M_0} \end{bmatrix} + qS\begin{bmatrix} -C_{L_\alpha} \\ \bar{c}C_{M_\alpha} \end{bmatrix}\theta_T \\ &+ \frac{qS\bar{c}}{2U_0}\begin{bmatrix} -C_{L_{\dot\alpha}} & -\ell C_{L_{\dot\alpha}} \\ \bar{c}C_{M_{\dot\alpha}} & \bar{c}\ell C_{M_{\dot\alpha}} \end{bmatrix}\begin{Bmatrix} \ddot h \\ \ddot\theta \end{Bmatrix} \\ &+ \frac{qS}{U_0}\begin{bmatrix} -C_{L_\alpha} & -\ell C_{L_\alpha} - \frac{\bar{c}}{2U_0}\left(C_{L_{\dot\alpha}} + C_{L_q}\right) \\ \bar{c}C_{M_\alpha} & \bar{c}\ell C_{M_\alpha} - \frac{\bar{c}}{2U_0}\left(C_{M_{\dot\alpha}} + C_{M_q}\right) \end{bmatrix}\begin{Bmatrix} \dot h \\ \dot\theta \end{Bmatrix} \\ &+ qS\begin{bmatrix} 0 & -C_{L_\alpha} \\ 0 & C_{M_\alpha} \end{bmatrix}\begin{Bmatrix} h \\ \theta \end{Bmatrix} + \frac{qS\bar{c}}{2U_0}\begin{bmatrix} -C_{L_{\dot\delta}} \\ \bar{c}C_{M_{\dot\delta}} \end{bmatrix}\dot\delta + qS\begin{bmatrix} -C_{L_\delta} \\ \bar{c}C_{M_\delta} \end{bmatrix}\delta \\ &- \frac{qS}{U_0}\begin{bmatrix} -\frac{\bar{c}}{2U_0}C_{L_{\dot\alpha}} & -C_{L_\alpha} \\ \frac{\bar{c}}{2U_0}C_{M_{\dot\alpha}} & \bar{c}C_{M_\alpha} \end{bmatrix}\begin{Bmatrix} \dot w_g \\ w_g \end{Bmatrix} \end{aligned} \tag{17}$$

Complete BACT Equations of Motion

Combining the generalized forces, Eqns (11) and (17), with Eqn (9) results in the complete equations of motion for the BACT system. The general form of the equations can be expressed as

$$\begin{aligned} &\left(M_s - M_a\right)\ddot q + \left(D_s - D_a\right)\dot q + \left(K_s - K_a\right)q \\ &\qquad = Q_0{}^e + Q_T\theta_T + M_g g\cos\theta_T \\ &\qquad\quad + B_2\ddot\delta + B_1\dot\delta + B_0\delta + Ew \end{aligned} \tag{18}$$

where q is the vector of generalized coordinates, w is the vector of disturbance inputs, and the definitions of the other symbols can be readily determined by comparison with Eqns (9), (11), and (17).

Notice that the effect of the aerodynamic forces is to modify the mass, damping, and stiffness properties of the system. It is this aerodynamic coupling that is the essential feature of aeroelastic systems and leads to the flutter instability.

Also note that there are three terms in the equations that are constant, assuming the turntable angle is fixed. These terms determine the static equilibrium of the system.

Equilibrium Solution and Perturbation Equations

The static equilibrium of the BACT system is obtained by setting all time derivatives in Eqn (18) to zero and solving for the generalized coordinates. Doing so results in the following expression.

$$\begin{aligned} q_0 = \left(K_s - K_a\right)^{-1}\Big(&Q_0{}^e + Q_T\theta_T \\ &+ M_g g\cos\theta_T + B_0\delta_0\Big) \end{aligned} \tag{19}$$

The subscript on the generalized coordinate vector is used to indicate static equilibrium. The subscript on the control input is used to denote its static value (i.e., bias).

The generalized coordinates can be expressed as the sum of the static (or equilibrium) part, q_0, and a perturbation part, $\tilde{q}$,

$$q = q_0 + \tilde{q} \tag{20}$$

The control input can be expressed as the sum of the bias or static part, δ_0, and the time varying or dynamic part, $\tilde{\delta}$.

$$\delta = \delta_0 + \tilde{\delta} \tag{21}$$

Substituting Eqns (20) and (21) into Eqn (18), using the fact that q_0, θ_T, and δ_0 are constant and eliminating the constant terms by using Eqn (19) results in the perturbation equations of motion for the BACT system as shown in Eqn (22).

$$\begin{Bmatrix} \ddot{\tilde{q}} \\ \dot{\tilde{q}} \end{Bmatrix} = \begin{bmatrix} -(M_s - M_a)^{-1}(K_s - K_a) & -(M_s - M_a)^{-1}(D_s - D_a) \\ I & 0 \end{bmatrix} \begin{Bmatrix} \dot{\tilde{q}} \\ \tilde{q} \end{Bmatrix} + \begin{bmatrix} -(M_s - M_a)^{-1} B_2 \\ 0 \end{bmatrix} \ddot{\tilde{\delta}} + \begin{bmatrix} -(M_s - M_a)^{-1} B_1 \\ 0 \end{bmatrix} \dot{\tilde{\delta}} + \begin{bmatrix} -(M_s - M_a)^{-1} B_0 \\ 0 \end{bmatrix} \tilde{\delta} + \begin{bmatrix} -(M_s - M_a)^{-1} E \\ 0 \end{bmatrix} w \tag{22}$$

While the form of the equations that appear in Eqn (18) describe the complete motion of the system, it is the form of the equations of motion presented in Eqn (22) that are most readily applicable to typical control system design methods. Note that even though Eqn (22) was derived for a single control surface, extension to multiple control surfaces is straight forward since there is no inertial coupling between the various control surfaces. There is, however, aerodynamic coupling between the control surfaces due to their close proximity to each other. The form of the aerodynamic force expressions allows this coupling to be approximated within the stability and control derivative terms. This can be done by altering the derivative values to account for control surface biases. Perturbation effects, however, are ignored in this approach.

Numerical Model Parameters

A numerical form of the equations of motion of the BACT system was obtained by substituting numerical values for each parameter in the equations of motion developed above. Most of the parameter values were obtained from experimental data but some of the aerodynamic data was obtained from numerical analysis using computational aerodynamics.

The mass and inertia parameters were obtained by measuring the mass, stiffness, and damping properties of the various components of the BACT system. The geometric parameters (e.g., centers of gravity, shear center, sensor locations, and aerodynamic reference quantities) were also obtained directly from measurement of the BACT and PAPA components. The mass, stiffness, and damping parameter values used in the numerical form of the BACT equations of motion are presented in Table 1. The center of gravity and shear center were nearly coincident and located at the mid-chord point of the wing.

Table 1 - Mass, Stiffness, and Damping Parameters

Symbol	Description	Value	Units
m	mass (plunge generalized mass)	6.08	slug
I_θ	pitch inertia (pitch generalized mass)	2.80	slug-ft^2
K_h	plunge stiffness	2686	lb/ft
K_θ	pitch stiffness	3000	ft-lb
ω_h	in vacuo plunge frequency	21.01	rad/sec
ω_θ	in vacuo pitch frequency	32.72	rad/sec
ζ_h	plunge damping ratio	0.0014	-
ζ_θ	pitch damping ratio	0.0010	-
$s_{h\theta}$	plunge - pitch coupling	0.0142	slug-ft
$s_{h\delta_{TE}}$	plunge - TE coupling	0.00288	slug-ft
$s_{\theta\delta_{TE}}$	pitch - TE coupling	0.00157	slug-ft^2
$s_{h\delta_{US}}$	plunge - US coupling	0.00039	slug-ft
$s_{\theta\delta_{US}}$	pitch - US coupling	9.8e-05	slug-ft^2

The static aerodynamic parameters were determined from experimental data obtained from a previous wind-tunnel test in which the BACT wing was mounted on a force and moment balance. Force and moment data for various angles of attack and control surface positions were used to compute most of the stability and control derivatives using finite differences.

Sufficient experimental data was only available to quantify the trailing edge control surface and upper-spoiler aerodynamic characteristics. Available data for the lower-spoiler was not complete enough to characterize its aerodynamics. In addition, there was little data to account for aerodynamic coupling between the spoiler and trailing edge control. Therefore, the numerical model is limited to the trailing edge and

upper-spoiler surfaces with no aerodynamic coupling between controls (e.g., spoiler blanking the trailing edge control).

The dynamic derivatives (e.g., C_{M_q} and $C_{L_{\dot{\alpha}}}$) were obtained from computational aerodynamic analysis. Analytical values were used because they were available from models previously generated using ISAC. However, the dynamic derivatives associated with control surface deflection rate were not available from these models. The parameters that were not available were assumed to be zero.

The numerical values for the static and dynamic stability and control derivatives are presented in Table 2. These values are only valid at a single Mach number, 0.77, and a single dynamic pressure, 143 psf. The moment coefficients are referenced relative to the shear center that coincides with the mid-chord point of the wing. Finally, note that the expression for the generalized aerodynamic forces, Eqn (17), requires the selection of an angle of attack reference point, ℓ (i.e., the distance between the shear center and the point at which the angle of attack of the wing is measured). A parametric study found that the best correlation between the numerical model and experimental data resulted when the reference point was chosen to be the aerodynamic center.

Table 2 - Aerodynamic Parameters

Symbol	Description	Value	Units
C_{L0}	lift at zero angle of attack	0	-
C_{M0}	pitching moment at zero angle of attack	0	-
$C_{L\alpha}$	lift curve slope	4.584	per rad
$C_{M\alpha}$	moment curve slope	1.490	per rad
$C_{L_{\dot{\alpha}}}$	plunge damping due to angle-of-attack rate	-3.1064	per rad
C_{L_q}	plunge damping due to pitch rate	2.5625	per rad
$C_{M_{\dot{\alpha}}}$	pitch damping due to angle-of-attack rate	-2.6505	per rad
C_{M_q}	pitch damping due to pitch rate	-0.4035	per rad
$C_{L_{\delta_{TE}}}$	TE lift effectiveness	0.63	per rad
$C_{L_{\dot{\delta}_{TE}}}$	TE rate lift effectiveness	0	per rad
$C_{M_{\delta_{TE}}}$	TE moment effectiveness	-0.0246	per rad
$C_{M_{\dot{\delta}_{TE}}}$	TE rate moment effectiveness	0	per rad
$C_{L_{\delta_{US}}}$	US lift effectiveness	0.22	per rad
$C_{L_{\dot{\delta}_{US}}}$	US rate lift effectiveness	0	per rad
$C_{M_{\delta_{US}}}$	US moment effectiveness	0.0573	per rad
$C_{M_{\dot{\delta}_{US}}}$	US rate moment effectiveness	0	per rad
ℓ	distance between shear center and aerodynamic center	-0.175	$\%\,\bar{c}$
S	planform area	3.55	ft^2
$\bar{c}$	mean aerodynamic chord	1.33	ft

Actuator and Turbulence Models and the Output Equation

The equations of motion alone are not sufficient to describe the dynamic behavior of the BACT system. While the 2-DOF system structure is sufficient to describe the basic aeroelastic properties of the BACT system, additional elements are necessary to develop a model suitable for control system design.

The relative magnitude of the dynamic response is determined by the nature of the disturbance environment. This influences the control activity required to achieve the desired level of closed-loop performance. Therefore, a characterization of the turbulence environment in the TDT is needed, i.e., a turbulence model. The ability of the control surfaces to produce the desired activity is dependent on the dynamic response characteristics of the actuators including bandwidth, position and rate limits, and other nonlinearities. Therefore, characterizations of the actuator dynamics are also needed, i.e., actuator models. Finally, a set of measurement signals is required to provide the basis for feedback control. An output equation relating the generalized coordinates to the measurement variables is therefore required.

It is the combination of the actuator models, the turbulence model, output equation, and the aeroelastic equations of motion that will determine the degree to which a control system will be able to achieve a desired level of performance and robustness.

Actuator Models

Actuator models of the BACT wind-tunnel model were obtained from experimental data using a simple parameter estimation process.[11] The process selected the parameters of the second order actuator model shown in Eqn (23) to minimize the frequency response error over the frequency range of interest.

$$\frac{\delta(s)}{\delta_c(s)} = \frac{k\omega^2}{s^2 + 2\zeta\omega s + \omega^2} \tag{23}$$

Here k is a gain, and ω and ζ are frequency and damping, respectively. The parameter values resulting from the parameter estimation process are presented in Table 3.

Table 3 - BACT Actuator Model Parameters

Symbol	Description	Value	Units
k_{TE}	TE actuator gain	1.02	deg/deg
ζ_{TE}	TE damping ratio	0.56	-
ω_{TE}	TE frequency	165.3	rad/sec
k_{US}	US actuator gain	1.16	deg/deg
ζ_{US}	US damping ratio	0.85	-
ω_{US}	US frequency	164.0	rad/sec
k_{LS}	LS actuator gain	1.09	deg/deg
ζ_{LS}	LS damping ratio	0.76	-
ω_{LS}	LS frequency	168.4	rad/sec

Turbulence Model

A model of the turbulence environment within the TDT was developed using power spectrum data from reference 12. The model structure is that of a Dryden spectrum with the parameters adjusted to approximate the desired power spectral density. Equation (24) shows the form of the turbulence model and Table 4 presents a range of values for the turbulence model parameters.

$$\frac{w_g(s)}{\eta_g(s)} = \frac{2\pi\sqrt{\alpha\beta}}{\gamma} \frac{\left(s + \frac{2\pi}{\sqrt{\beta}}\right)}{\left(s^2 + \frac{4\pi}{\sqrt{\gamma}}s + \frac{4\pi^2}{\gamma}\right)} \tag{24}$$

where $\beta = \beta_p\left(\frac{2\pi L_t}{V}\right)^2$ and $\gamma = \gamma_p\left(\frac{2\pi L_t}{V}\right)^2$.

Note that the parameter values are based on data collected in an air medium, not the medium in which the BACT was tested (i.e., R-12) and so the reference speed, V, corresponds to a different Mach number. No data at the appropriate operating conditions is available. A reference speed close to the airspeed associated with a particular test condition was used for analysis and design purposes.

Table 4 - TDT Turbulence Model Parameters

	Reference Speed (fps)			
Symbol	100	200	300	400
α	0.01	0.025	0.007	0.082
β_p	0.477	0.475	0.521	0.667
γ_p	0.546	0.464	0.497	0.533
L_t	3.261	3.71	3.391	4.163

Output Equation

The BACT system has four accelerometers, one mounted in each corner of the rectangular wing. These accelerometers sense vertical acceleration measured in g's, positive up (opposite to the sign convention for plunge, h). The acceleration at any point on the BACT wing, excluding control surfaces, has two components as shown in Eqn (25).

$$\ddot{z}(x) = \frac{-\left(\ddot{h} + d\ddot{\theta}\right)}{g} \tag{25}$$

where h and θ are the generalized coordinates, d is the chordwise distance from the reference point to the shear center, and g is the gravitational acceleration. Table 5 presents the chordwise distance (positive aft) between the shear center and the accelerometer for each of the four accelerometers -- leading edge inboard (LEI), leading edge outboard (LEO), trailing edge inboard (TEI), and trailing edge outboard (TEO).

Table 5 - Accelerometer Locations

Accelerometer Location	d_{LEI}	d_{LEO}	d_{TEI}	d_{TEO}
Distance (ft)	-0.599	-0.599	0.433	0.420

All the components described above were combined to form the complete numerical model of the BACT system. The following section addresses a variety of analyses that were performed to assess the accuracy and validity of the model.

Validation of Numerical Model

There are many ways to assess various aspects of the validity of the BACT numerical model. In this section a few comparisons are made between the properties of the numerical model and the actual BACT wind-tunnel model. These assessments can be broken down into two categories -- static properties and dynamic properties. The static properties assess the characteristics of the equilibrium solutions. The dynamic properties assess the key response characteristics of the system in the context of flutter behavior and control system design.

Static Properties

The equilibrium position (pitch and plunge) of the BACT system depends on the turntable angle and wind-tunnel operating conditions and represents a balance

between the elastic and aerodynamic forces acting on the wing. Good agreement between the equilibrium position of the wind-tunnel model and the equilibrium solution of the numerical model would indicate that the stiffness (structural and aerodynamic) and control surface effectiveness properties are well modeled.

Two variables that were recorded during the wind-tunnel tests are turntable angle and pitch angle (plunge position was not measured). In addition, the test conditions (i.e., Mach number, dynamic pressure, and control surface positions) were recorded. Using the later quantities in Eqn (19), one can determine the equilibrium pitch and plunge position of the BACT system for comparison with experiment.

Table 6 presents the computed and measured pitch angle for a small representative set of test conditions. The error in equilibrium pitch angle is less than 5 percent for all but one point. In addition, the trends are consistent; increasing the turntable angle increases the pitch angle, deflecting the upper-spoiler decreases the pitch angle, and deflecting the trailing edge control downward decreases the pitch angle.

The size of the pitch angle increments due to turntable angle and spoiler deflection are also very similar. The main discrepancy is in the pitch angle increment due to trailing edge control deflection. The pitch angle change due to trailing edge control from the experimental data is five times higher than from the numerical model.

Dynamic Properties

A major concern in using the numerical model for control system design is the ability of the model to accurately represent the transition to flutter including the frequency and dynamic pressure of the flutter onset. Another concern is the fidelity of the model from a frequency response perspective because of the relationship between the frequency response and the structure of the control system. Finally, the level of response due to turbulence is an important issue since the maximum level of control activity depends directly on the level of response of the wind-tunnel model to turbulence. Each of these properties will be reviewed and compared with experimental data (and numerical models generated with ISAC where possible) to assess the validity of the numerical model.

Flutter Properties

The BACT wind-tunnel model experienced flutter in the TDT at a dynamic pressure of approximately 148 psf at a Mach number of 0.77. The flutter dynamic pressure for the numerical model is 150.8 psf, an difference of 1.9 percent. ISAC generated models indicate flutter occurs between 156 and 163 psf.

The flutter frequency of the BACT wind-tunnel model is approximately 4 hertz. At the same operating condition the flutter frequency of the numerical model is 4.16 hertz, a 4.0 percent difference. ISAC generated models indicate the flutter frequency to be approximately 4.22 hertz.

In terms of the flutter dynamic pressure and frequency at the Mach number for which aerodynamic data was available, the numerical model of the BACT system gives excellent results.

Transfer Function Comparisons

One of the most important measures of model fidelity for control system design is the frequency response. In order to effectively design a control system to stabilize a flutter mode the design model must accurately characterize the dynamic behavior of the aeroelastic system over a fairly wide range of dynamic pressures from stability to neutral stability to instability.

Figures 6 and 7 show comparisons between the frequency responses for the numerical model and the actual wind-tunnel model. The operating condition corresponds to subsonic Mach number and a dynamic pressure of 125 psf, well below flutter. In Figure 6

Table 6 - Static Equilibrium Position Comparison

Mach Number	Dynamic Pressure (psf)	θ_T (deg)	δ_{TE} (deg)	δ_{US} (deg)	θ_{exp} (deg)	θ_{model} (deg)	$\Delta\theta$ (%)
.65	112	1.6	0	**0**	2.1	2.17	3.33
.65	115	1.6	0	**-10**	2.0	2.05	2.50
				$\Delta\theta\ (\delta_{US})$	0.1	0.12	
.70	126	1.6	**0**	0	2.4	2.28	-5.00
.70	126	1.6	**10**	0	2.0	2.20	10.0
				$\Delta\theta\ (\delta_{TE})$	0.4	0.08	
.77	120	**1.4**	0	0	2.0	1.95	-2.50
.77	120	**4.5**	0	0	6.0	6.27	4.50
				$\Delta\theta\ (\theta_T)$	-4.0	-4.32	

the output is the trailing edge accelerometer and the input is the trailing-edge control. In Figure 7 the output is the trailing-edge accelerometer and the input is the upper spoiler control. An ISAC-based model is also presented in Figure 6 for comparison. Recall that ISAC cannot model spoilers and so no ISAC comparison can be made in Figure 7. The frequency response comparisons for the other accelerometers are comparable to those shown here.

There is excellent correlation between the experimentally obtained frequency responses and those of the numerical model. The model clearly captures the key aspects of the dynamic response of the BACT system at the subcritical dynamic pressure of 125 psf. There are, however, slight discrepancies in the frequency of the magnitude peak near 3.5 hertz and in the phase characteristics of both responses.

Open-Loop RMS Accelerations

It is important for the numerical model to accurately characterize the response of the system to disturbances since disturbance response determines the control activity required to achieve the desired level of closed-loop performance. The disturbance source for the BACT system is wind-tunnel turbulence. One measure of the degree to which the numerical model characterizes the turbulence is rms acceleration.

Table 7 presents a comparison of the rms trailing edge inboard accelerations at two dynamic pressures. The comparison is based on normalizing the dynamic pressure by the associated flutter dynamic pressure, q_f. Normalization is needed because of the differences in the flutter dynamic pressure for the experimental data and the numerical model. The reference speed used to scale the turbulence model is 400 fps and is consistent with the speed of the flow in the wind-tunnel.

Note that there is a Mach number mismatch between the experimental data and the model-based data since the aerodynamic parameter values in the numerical model are based on data collected at Mach 0.77 and the experimental data was obtained for Mach numbers of 0.63 and 0.71, respectively. The good agreement in the response level implies that the numerical model can be used to assess rms response.

Comments

Based on the accuracy of the flutter properties, the subcritical frequency responses, and rms disturbance response, it is reasonable to expect the model to accurately characterize the dynamic response of the BACT system over a wide range of operating conditions and is appropriate for control system design. Nevertheless, the dynamic behavior of the numerical model near flutter has not been directly verified and could deviate from the actual system despite the similarities presented above.

In addition, the discrepancies identified above should be taken into account during control system design and dynamic analysis. In particular, the static analysis

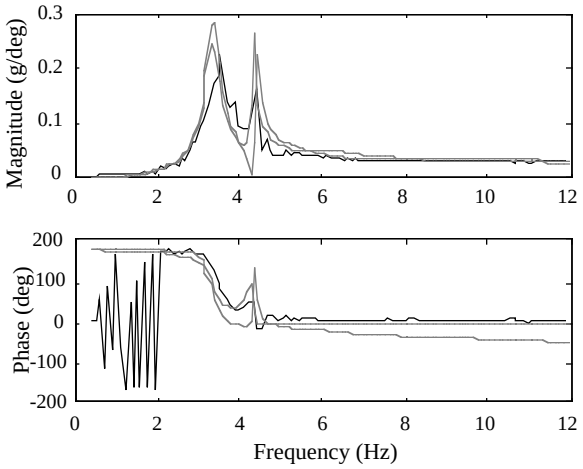

Figure 6 - Frequency response comparison for trailing-edge inboard accelerometer due to trailing edge control: q = 125 psf.
(solid - exp, dash - model, dot - ISAC)

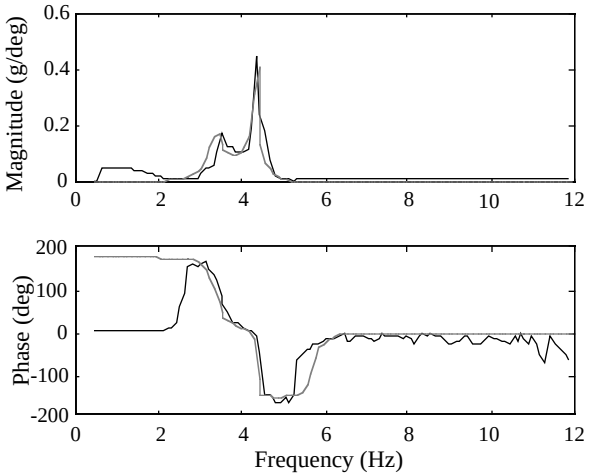

Figure 7 - Frequency response comparison for trailing-edge inboard accelerometer due to upper spoiler control: q = 125 psf.
(solid - exp, dash - model)

Table 7 - Comparison of RMS Trailing-Edge Acceleration

q_{norm} (psf)	RMS Trailing Edge Acceleration (g)		% Error
	Experiment	Model	
$0.75*q_f$	0.0207	0.0188	-9.2
$0.90*q_f$	0.0340	0.0350	2.9

supports the possibility that the pitch effectiveness of the trailing edge control surface in the numerical model may be somewhat low. There are also slight peak frequency and phase differences between the numerical model and the experimental data in the frequency response plots that could represent uncertainty in pole and zero locations of the numerical model.

Concluding Remarks

The dynamic model of the Benchmark Active Control Technology (BACT) wind-tunnel model presented herein has many advantages over a purely numerically derived model. It is analytical and parametric in nature and therefore lends itself to sensitivity and uncertainty analysis. Since the aerodynamic effects are represented in derivative form experimental data can readily be substituted for analysis-based data. A major advantage of the modeling approach is that it allows experimental stability and control derivative data to be used to model spoiler effects not possible with the traditional modeling method. The modular form of the model also allows various components of the model to be modified or replaced. This is very useful in cases where actuator models and turbulence models are modified or updated.

A Matlab®/Simulink® implementation of the wind-tunnel model, actuator models, turbulence model, and digital controller effects has been developed for the purpose of evaluating and analyzing the dynamic behavior of the BACT system. It has been used by several researchers to assist in the design and analysis of flutter suppression controllers. A variety of classical, H_∞, μ-synthesis, neural network, and adaptive controllers have been designed using the numerical model and have been successfully tested in the Langley Transonic Dynamics Tunnel.

The BACT model and test data are also being developed as a case study package for educational use. The relatively simple structure of the BACT system coupled with the availability of extensive and detailed experimental data make the BACT an excellent candidate for the study of dynamics and control of aeroelastic systems.

Acknowledgment

The author wishes to acknowledge Rob Scott, Sheri Hoadley, Carol Wieseman, Robert Bennett, Robert Sleeper, and the entire BACT team without whose help this work could not have been accomplished.

References

[1] Durham, M.H.; Keller, D.F.; Bennett, R.M.; and Wieseman, C.D.: A Status Report on a Model for Benchmark Active Controls Testing. AIAA Paper No. 91-1011.

[2] Bennett. R.M.; Eckstrom, C.V.; et al..: The Benchmark Aeroelastic Models Program - Description and Highlights of Initial Results. NASA TM-104180, Dec. 1991.

[3] Wieseman, C.D.; Hoadley, S.T.; and McGraw, S.M.: On-Line Analysis Capabilities Developed to Support Active Flexible Wing Wind-Tunnel Model. *Journal of Aircraft.* Vol. 23, No. 1. pp. 39-44. Jan.-Feb. 1995.

[4] Adams, W.M.: ISAC: A Tool for Aeroservoelastic Modeling and Analysis. NASA TM-109031. December, 1993.

[5] Rivera, Jr., J.A.; Dansberry, B.E.; et al..: NACA 0012 Benchmark Model Experimental Flutter Results with Unsteady Pressure Distributions. AIAA Paper No. 92-2396. 33rd AIAA/ASME/ ASCE/AHS/ASC Structures, Structural Dynamics, and Materials Conference. Dallas, TX, April 1992.

[6] Baals, D.D. and Corliss, W.R.: Wind Tunnels of NASA. pp. 79-81. NASA SP-440.

[7] Rivera, Jr., J.A.; Dansberry, B.E.; Durham, M.H.; Bennett, R.M.; and Silva, W.A.: Pressure Measurements on a Rectangular Wing with a NACA 0012 Airfoil During Conventional Flutter. NASA TM-104211, July 1992.

[8] Bisplinghoff, R.L. and Ashley, H.: *Principles of Aeroelasticity.* Dover Publications, Inc., New York. 1962.

[9] Waszak, M.R. and Schmidt, D.K.: Flight Dynamics of Aeroelastic Vehicles. *Journal of Aircraft.* pp. 563-571. Vol. 25, No 6. June 1988.

[10] Dansberry, B.E.; Durham, M.H.; Bennett, R.M.; Turnock, D.L.; Silva, W.A.; and Rivera, Jr., J.A.: Physical Properties of the Benchmark Models Program Supercritical Wing. NASA TM-4457. September 1993.

[11] Waszak, M.R. and Fung, J.: Parameter Estimation and Analysis of Actuators for the BACT Wind-Tunnel Model. AIAA Paper No. 96-3362. AIAA Atmospheric Flight Mechanics Conference. San Diego, CA. July 29-31, 1996.

[12] Sleeper, R.K.; Keller, D.F.; Perry III, B.; and Sanford, M.C.: Characteristics of Vertical and Lateral Tunnel Turbulence Measured in Air in the Langley Transonic Dynamics Tunnel. NASA TM-107734. March 1993